CO-bridged H-Cluster intermediates in the catalytic mechanism of [FeFe]-hydrogenase CaI.

Michael W. Ratzloff,[1] Jacob H. Artz,[1] David W. Mulder,[1] Reuben T. Collins,[2] Thomas E. Furtak,[2] and Paul W. King[1]*

[1] Biosciences Center, National Renewable Energy Laboratory, Golden, CO 80401, USA

[2] Physics Department, Colorado School of Mines, Golden, CO 80401, USA

ABSTRACT: The [FeFe]-hydrogenases ([FeFe] H_2ases) catalyze reversible H_2 activation at the H-cluster, which is composed of a $[4Fe\text{-}4S]_H$ subsite linked by a cysteine thiolate to a bridged, organometallic [2Fe-2S] ($[2Fe]_H$) subsite. Profoundly different geometric models of the H-cluster redox states that orchestrate the electron/proton transfer steps of H_2 bond activation have been proposed. We have examined this question in the [FeFe] H_2ase I from *Clostridium acetobutylicum* (CaI) by Fourier-transform infrared (FTIR) spectroscopy with temperature annealing and H/D isotope exchange to identify the relevant redox states and define catalytic transitions. One-electron reduction of H_{ox} led to formation of $H_{red}H^+$ ($[4Fe\text{-}4S]_H^{2+}$-Fe^I-Fe^I) and H_{red}' ($[4Fe\text{-}4S]_H^{1+}$-Fe^{II}-Fe^I), with both states characterized by low frequency μ-CO IR modes consistent with a fully bridged $[2Fe]_H$. Similar μ-CO IR modes were also identified for $H_{red}H^+$ of the [FeFe] H_2ase from *Chlamydomonas reinhardtii* (CrHydA1). The CaI proton-transfer variant C298S showed enrichment of an H/D isotope-sensitive μ-CO mode, a component of the hydride bound H-cluster IR signal, H_{hyd}. Equilibrating CaI with increasing amounts of NaDT, and probed at cryogenic temperatures, showed $H_{red}H^+$ was converted to H_{hyd}. Over an increasing temperature range from 10 to 260 K catalytic turnover led to loss of H_{hyd} and appearance of H_{ox}, consistent with enzymatic turnover and H_2 formation. The results show for CaI that the μ-CO of $[2Fe]_H$ remains bridging for all of the "H_{red}" states and that $H_{red}H^+$ is on pathway to H_{hyd} and H_2 evolution in the catalytic mechanism. This provides a blueprint for designing small molecule catalytic analogs.

Introduction

The [FeFe] hydrogenases ([FeFe] H_2ase) catalyze the reversible activation of hydrogen (H_2) with the catalytic site H-cluster, an iron-sulfur cofactor that functions to couple proton and electron transfer to the catalytic activation of H_2.[1-3] The H-cluster [4Fe-4S] cubane subsite ($[4Fe\text{-}4S]_H$) is linked to a diiron subsite ($[2Fe]_H$) via a cysteine-derived thiolate bridge (Figure 1).[4-5] Both the proximal (Fe_p) and distal (Fe_d) iron atoms of $[2Fe]_H$ (designated based on position relative to $[4Fe\text{-}4S]_H$) are coordinated by terminal carbonyl (CO) and cyanyl (CN) ligands, and a bridging μ-CO. $[2Fe]_H$ is further bridged by an azadithiolate (adt) ligand[6-8] that functions in proton-transfer between the H-cluster and the conserved proton-transfer pathway to the [FeFe] H_2ase surface (Figure 1).[9-11] These attributes of the H-cluster and surrounding environment are designed to match favorable redox potentials with facile proton-exchange to enable the rapid catalytic turnover observed by [FeFe] H_2ases.[12]

Spectroscopic analyses of [FeFe] H_2ases with theoretical models of the H-cluster are providing insights on how design elements function to support the required proton and electron-transfer steps for catalysis.[13-16] Chemically synthesized active sites incorporating $[2Fe]_H$ subsites with oxo (odt) or propyl (pdt) groups as the bridgehead atom,[6, 17-19] as well as site-directed mutagenesis of proton-transfer residues,[20-21] establishes the role of adt in mediating proton-transfer at $[2Fe]_H$.[22] Moreover, the odt, pdt, and adt derivatives populate different redox states, implicating that facile proton exchange at the H-cluster supports proton-coupled electron transfer (PCET) driven redox transitions during catalysis.[23]

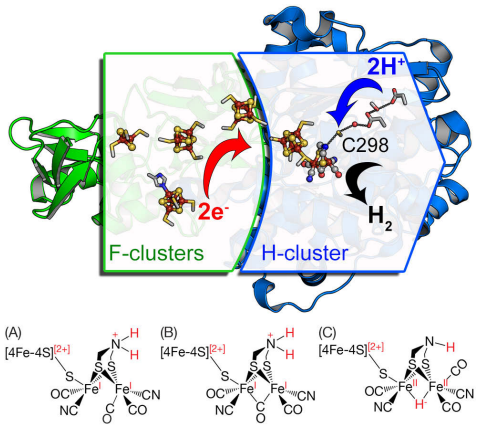

Figure 1. **Top**. Structural representation of *Clostridium acetobutylicum* [FeFe] H_2ase I (CaI) showing the convergence of electron (e^-) and proton (H^+) transfer pathways. The F-cluster (green) and H-cluster (blue) domains are based on the crystal structure of *Clostridium pasteurianum* [FeFe] H_2ase I (CpI), PDB 3C8Y.[24] **Bottom**. Models of the H-cluster $H_{red}H^+$ state. **A**. The $[2Fe]_H$ μ-CO shifted to a terminal position, with an open coordination site at Fe_d.[16, 25] **B**. The $[2Fe]_H$ retains a μ-CO, with an open coordination site at Fe_d.[7, 13, 22, 26] **C**. The $[2Fe]_H$ with a μ-H^-, and a CO occupying the Fe_d open coordination site.[27] For each model, one-electron reduction of $H_{red}H^+$ maintains the same $[2Fe]_H$ geometry, but $[4Fe\text{-}4S]_H$ oxidation state changes from 2^+ to 1^+ (note: the nomenclature and amine protonation state of $[2Fe]_H$ also varies in each model).[16, 22, 27-28]

Pursuant to the DOE Public Access Plan, this document represents the authors' peer-reviewed, accepted manuscript. The published version of the article is available from the relevant publisher.

Collectively these studies have led to fundamentally different models for both geometric structures and catalytic mechanisms. For example, three distinct models have been proposed for the structure of H_{red} (i.e., $[4Fe\text{-}4S]_H^{2+}$ with $[2Fe]_H$ in different oxidation states) that profoundly differ in the geometry of the μ-CO and the occupation of the open coordination site on the distal Fe (Fe_d) atom of $[2Fe]_H$ (Figure 1).[13, 16, 25, 27, 29-30] The different models alter the μ-CO geometry relative to Fe_d, to be either fully bridged or completely terminal and have mechanistic implications. In the latter case, the apical CO on Fe_d can be accompanied by protonation to form a μ-H, supporting a conclusion that H_{red} (and H_{sred}) are both off-path, non-catalytic states.[27] Although the electronic structures of H-cluster states have been determined by EPR and FTIR spectroscopy, the protonation states of $[2Fe]_H$ (including the bridging amine) are much less resolved.[22, 29, 31]

The mechanistic models of [FeFe] H_2ases have largely been derived from studies of the minimal enzyme from *Chlamydomonas reinhardtii* (CrHydA1), and it is not yet clear how the structural diversity of [FeFe] H_2ases contributes differences in H-cluster reactivities. Compared to CrHydA1, more complex [FeFe] H_2ases possess additional FeS clusters or F-clusters (Figure 1) that mediate electron transfer between the H-cluster and physiological redox partners. The F-clusters not only determine the energy landscape of electron transfer, but affect the H-cluster electronic properties.[32-34] F-clusters have been implicated to effect catalytic bias between H_2-uptake and H_2-evolution[35] and in fine-tuning of the HOMO/LUMO interactions within the H-cluster.[31] Thus, determining the nature of H-cluster redox states across [FeFe] H_2ase structural diversity can lead to new insights and refine redox state assignments. In addition, H-cluster synthetic analogs lack the catalytic performance of [FeFe] H_2ases, suggesting the protein has a critical function in fine tuning of the electron and proton-transfer steps.[36-38]

We have studied the structural and electronic properties of the H-cluster in the bacterial [FeFe] H_2ase I from *Clostridium acetobutylicum* (CaI, Figure 1) by Fourier-transform infrared (FTIR) spectroscopy. The CO and CN ligands give rise to strong IR modes that can be used to distinguish different H-cluster redox state geometries, such as the μ-CO ligand specific to the 1850-1800 cm^{-1} region. By combining temperature annealing and H/D-isotope exchange we were able to correlate temperature and H/D isotope effects on redox induced shifts in the IR spectrum to geometrical changes in $[2Fe]_H$ under turnover. The results resolve structural differences important to defining a mechanistic model for H_2 catalysis and demonstrate that the bridging CO ligand geometry is a critical component of reduced state H-cluster transitions towards achieving fast, efficient catalysis.

Results and Discussion

Oxidized CaI. To assign the IR spectra of CaI to H-cluster oxidation states, CaI was initially prepared under reduction with sodium dithionite (NaDT) and then allowed to turnover at 295 K until oxidized (referred to as "auto-oxidized").[39] The IR spectrum of auto-oxidized CaI in either H_2O or D_2O buffer (Figure S1) shows the well-defined spectrum of oxidized [FeFe] H_2ases (H_{ox}), with CN bands 2082 and 2070 cm^{-1}, terminal CO bands at 1969, 1946 cm^{-1}, and a μ-CO band at 1800 cm^{-1}. Under certain conditions, there was an upshift in the H_{ox} spectrum (Figure S1C and S1D) with CN bands at 2090 and 2075 cm^{-1}, terminal CO bands at 1975 and 1953 cm^{-1}, and a μ-CO band at 1809 cm^{-1} (summarized in Table S1). Similar shifts have been observed for the H_{ox} spectrum of CrHydA1 prepared under neutral to acidic pH and have been assigned to a protonated form of the H_{ox} state termed $H_{ox}H^+$.[15] Consistent with this assignment, we observed a lower steady-state population of $H_{ox}H^+$ when CaI was equilibrated in D_2O (i.e., $H_{ox}D^+$) at pD 8, without any accompanying H/D isotope-sensitive shifts in the IR frequencies (Figure S1).

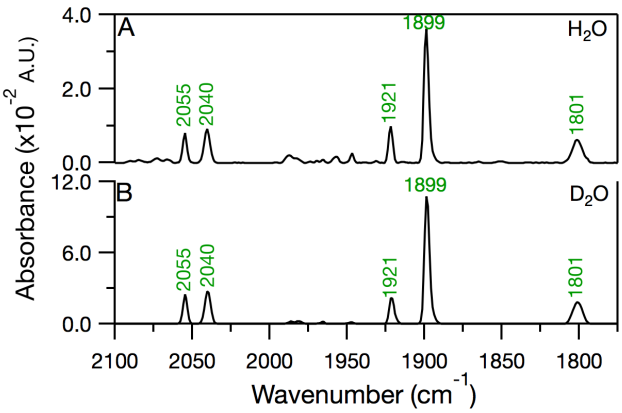

Figure 2. Cryogenic FTIR spectrum of H/D-isotope exchanged, reduced CaI. An aliquot of 246 μM CaI was equilibrated in either H_2O (**A**) or D_2O (**B**) buffer, allowed to auto-oxidize at 295 K, then reduced with 25 mM NaDT at 295 K. The IR spectra were collected at 13 K. Spectra are colored as $H_{red}H^+$, green.

The IR Spectrum and $[2Fe]_H$ Geometry of $H_{red}H^+$ in CaI and CrHydA1. We next examined the IR spectra of reduced CaI under a variety of NaDT conditions, in either H_2O or D_2O buffers. As shown in Figure 2, oxidation of CaI in both solvents produced a uniform H_{ox} spectrum that lacked $H_{ox}H^+$. After reduction with excess NaDT (25 mM) at 295 K, the spectrum of CaI was collected at 13 K. This spectrum again was composed of a single species, but with a significant down-shift of the CN and CO bands (Figure 2) that have been assigned to $H_{red}H^+$ in CrHydA1.[13, 16, 29] The CN bands in CaI at 2055 and 2040 cm^{-1} coincide with clearly defined terminal CO bands at 1921 and 1899 cm^{-1}, and a distinct μ-CO band at 1801 cm^{-1}. This spectrum is most similar to the "H^*_{red}" assigned to a $[4Fe\text{-}4S]^{2+}$-Fe^I-Fe^I H-cluster with a mono-protonated adt in the putative H_2 sensing [FeFe] H_2ase, HydS, from *Thermotoga maritima*,[30] and H_{red} of CrHydA1 observed by Silakov et al.[29], but differs from H_{red} of DdH that apparently lacks a μ-CO (Figure 1A).[40-41] NaDT treatment of CaI performed in D_2O at 13 K also produced a predominantly μ-CO bridged H_{red} spectrum without any observable H/D isotope shifts. The FTIR spectra of reduced CrHydA1 also showed distinct μ-CO bands coinciding with enrichment of $H_{red}H^+$ and other reduced species (Figures S2-S4). These results for both CrHydA1 and CaI show that the terminal coordination site of Fe_d is not occupied by a H-ligand, which would produce a downshift in the μ-CO compared to the spectrum collected in H_2O.[13] Altogether the IR spectrum of reduced CaI and CrHydA1 are most consistent with the H-cluster structural model for $H_{red}H^+$ with a fully bridging CO, presented in Figure 1B.

Proton-Transfer at $[2Fe]_H$ and Formation of H_{hyd} in CaI. The 1-electron reduction of H_{red} produces a mixture of two different products either H_{hyd} which has a hydride bound to the H-cluster, or H_{sred}. The H_{hyd} state is characterized by a distinctive IR spectrum that exhibits an H/D-isotope sensitive μ-CO band

Pursuant to the DOE Public Access Plan, this document represents the authors' peer-reviewed, accepted manuscript. The published version of the article is available from the relevant publisher.

due to the back-bonding effect of a H^- ligand terminally bound to Fe_d of $[2Fe]_H$.[13, 22] The H_{hyd} state has been identified in both natural and synthetically matured (i.e., $[2Fe]_H$ with an adt or odt synthetic ligand) CrHydA1 and DdH.[42-43] To identify the H_{hyd} intermediate in CaI we used an enrichment strategy based on changing a conserved Cysteine (C298, corresponding to CpI C299) to a Serine which disrupts proton-transfer to adt, and traps the H-cluster in the H_{hyd} state.[13, 44]

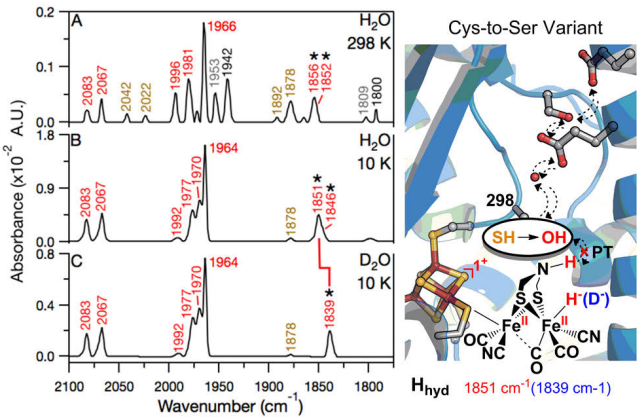

Figure 3. FTIR spectra of the NaDT reduced CaI C298S variant. **A**. Reduced with 10 mM NaDT, pH 8 at 295 K. **B**. Reduced with 10 mM NaDT in H_2O, pH 8 at 10 K. **C**. Reduced with 10 mM NaDT in D_2O, pD 8 at 10 K. Spectra are colored as H_{ox}, black; $H_{ox}H^+$, gray; H_{sred}, brown; and H_{hyd}, red. H/D-isotope sensitive peaks are noted with (∗). Samples at 1.2 mM. The scheme on the right depicts the SH-to-OH side chain modification near the H-cluster and disruption of proton-transfer (PT) pathway (dotted arrows) in the Cys-to-Ser variant causing enrichment of H_{hyd}.

Figure 3 shows the IR spectra of the CaI variant C298S reduced with NaDT. The spectrum of the as-prepared sample (Figure S4) showed a complex mixture of states, that after reduction with NaDT resolved into two states at 295 K (Figure 3A). The state with CN bands at 2083 and 2067 cm^{-1}, terminal CO bands at 1996, 1981, 1966 cm^{-1}, and μ-CO bands at 1856 and 1852 cm^{-1} strongly resembles the H_{hyd} spectra of CrHydA1 and Ddh.[13, 42] Confirmation that $[2Fe]_H$ has a terminally bound hydride was evident from a shift in the μ-CO band frequency of the sample prepared in H_2O versus D_2O (Figure 3B versus 3C). This 7-12 cm^{-1} downshift of the μ-CO band in the deuterated versus hydrogenated sample is due to the *trans*-effect of the terminal hydride bound to Fe_d.[13] The H_{hyd} spectrum of C298S otherwise has identical terminal CN and CO band frequencies.

H_{sred} Signal in CaI C298S. The NaDT reduced CaI C298S at 295 K (Figure 3A) also showed a second slightly weaker signal with CN bands at 2042, 2022 cm^{-1}, terminal CO bands at 1892 and 1878 cm^{-1}, and a μ-CO band at 1781 cm^{-1}, identified from the as-prepared sample, that can be assigned to this signal (Figure S4). These bands correspond well to the H_{sred} signal of CrHydA1 (2067, 2027, 1953, 1917, 1881 cm^{-1})[16] and the H_{sred} signal identified in *T. maritima* HydS (2047, 2013, 1900, 1861 and 1751 cm^{-1}).[30] The large downshift (~40-100 cm^{-1}) of CN/CO bands relative to the H_{hyd} signal (Figure 3A and Figure S4; brown versus red labelled bands) is indicative of reduction of $[2Fe]_H$ and the presence of H_{sred}.[13, 16, 22] Thus, the altered proton-transfer kinetics in CaI C298S favor the accumulation of electrons on the H-cluster, which in this enzyme results in an apparent equilibrium (tautomerization) between H_{sred} and H_{hyd}.[45] This is also evidenced by the H_{sred} peak at 1878 cm^{-1} in the 10 K samples that are enriched in H_{hyd} in Figure 3B.

An H/D Kinetic Isotope Effect on the Transition of $H_{red}H^+$ to H_{hyd}. The H/D isotope exchanged IR spectra of reduced CaI collected at 295 K demonstrate a mixture of states (Figure 4 and Figure S5). A comparison of Figure 4A to 4B shows a striking difference in the relative amounts of $H_{red}H^+$ and H_{red} in reduced CaI when prepared in H-enriched versus D-enriched buffers, with higher amounts in D_2O versus H_2O. The $H_{red}H^+ \rightarrow H_{hyd}$ step proceeds by a intramolecular proton-transfer, and we hypothesize that slower kinetics in D_2O leads to accumulation of $H_{red}H^+/H_{red}$ over H_{hyd}.[23] Differential enrichment of $H_{red}/H_{red}H^+$ in D_2O versus H_2O would also be expected to occur since $H_{ox} \rightarrow H_{red}H^+$ proceeds by PCET on the reaction pathway to H_2 formation, which we have shown for CaI has a solvent kinetic isotope effect of 2.5.[23]

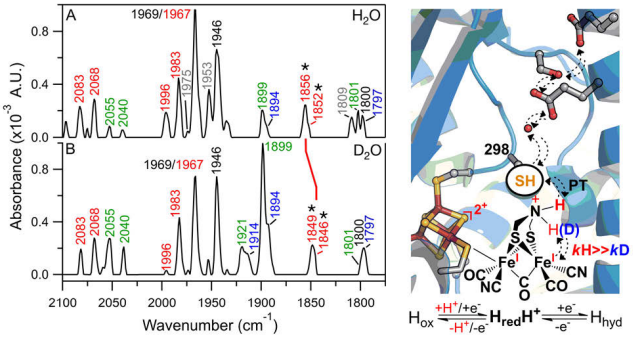

Figure 4. The 295 K FTIR spectra of native CaI. **A**. 100 mM NaDT in H_2O, pH 8. **B**. 100 mM NaDT in D_2O, pD 8. Spectra are color coded as: H_{ox}, black; $H_{ox}H^+$, gray; $H_{red}H^+$, green; H_{red}, blue; and H_{hyd}, red. H/D-isotope sensitive peaks are noted with (*). Spectra recorded at 295 K. The [CaI] was 1.6 mM. A model scheme of the $H_{ox} \rightarrow H_{hyd}$ conversion steps for CaI is shown on the right.

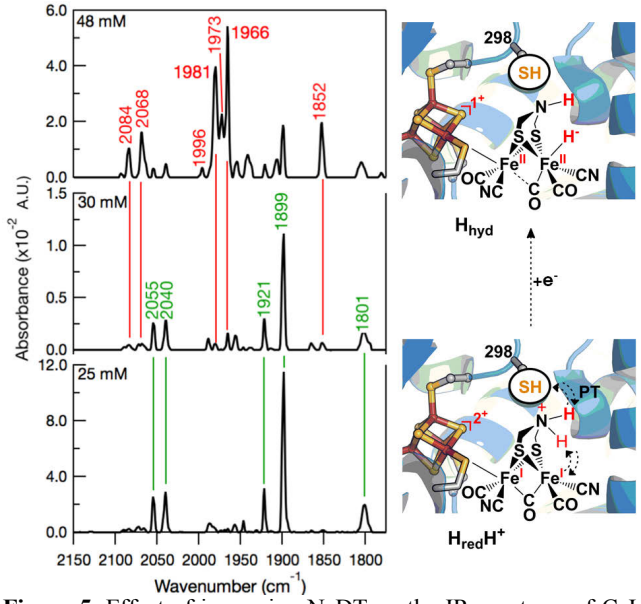

Figure 5. Effect of increasing NaDT on the IR spectrum of CaI. Auto-oxidized CaI was reduced with a gradually increasing concentration of NaDT (25 to 48 mM, bottom to top, respectively) and the IR collected at 13 K. The CN and CO bands of $H_{red}H^+$ (green) or H_{hyd} (red) are shown. The CaI concentrations were 1.7, 5.4, 3.6 mM, bottom to top. A scheme of the $H_{red}H^+ \rightarrow H_{hyd}$ H-cluster redox transition is shown on the right.

Pursuant to the DOE Public Access Plan, this document represents the authors' peer-reviewed, accepted manuscript. The published version of the article is available from the relevant publisher.

The Interconversion of $H_{red}H^+ \leftrightarrow H_{hyd}$ is a Catalytic Step in the Mechanism of CaI. Studies on CrHydA1 have led to different proposals on the geometric structures of $H_{red}H^+$ and H_{sred}, (Figures 1A-1C) and their roles in the catalytic mechanism. For CaI, the structure of $H_{red}H^+$ we have assigned from the H/D-isotope exchanged IR spectrum collected at 13 K (Figure 2) matches best to a bridged $[2Fe]_H$ geometry with a μ-CO (Figure 1B) and open Fe_d site for reversible H_2 activation.

To address in CaI whether $H_{red}H^+$ is either an on-path catalytic intermediate or a dead-end product, we examined the effect of addition of increasing amounts of NaDT on the steady-state equilibrium population of H-cluster redox states. Reduction of CaI with 25 mM NaDT produced a uniform $H_{red}H^+$ spectrum along with other minor components (Figure 5). Increasing the NaDT to 30 mM resulted in the appearance of the H_{hyd} signal (indicated by red lines in Figure 5). The intensity of the H_{hyd} signal and its proportion relative to $H_{red}H^+$, increased as the NaDT was increased from 30 to 48 mM. In fact, the increase in the H_{hyd} population coincided with a pronounced decrease in the level of $H_{red}H^+$. The implication of these results is that $H_{red}H^+$ and H_{hyd} are linked by a redox process, whereupon reduction of $H_{red}H^+$ by one-electron with transfer of an H^+ from adt results in formation of the terminal hydride on Fe_d of the H_{hyd} state (Figure 5, scheme on the right).

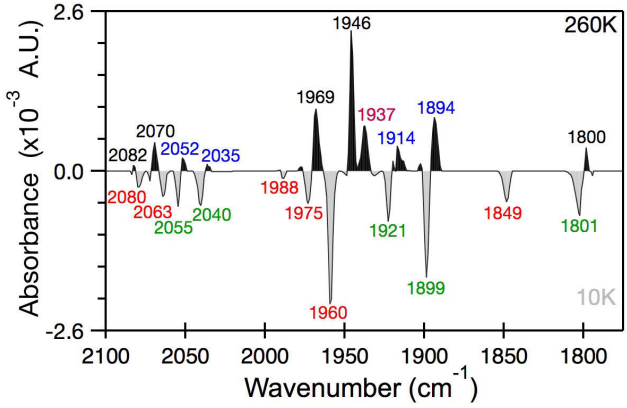

Figure 6. FTIR difference spectra of temperature-annealing changes in native CaI reduced with NaDT. CaI (2.8 mM) was reduced with 10 mM NaDT for 1 h at 278 K in H_2O, pH 8. The starting spectrum was collected at 10 K (bottom panel) and the sample temperature was increased (stepwise, see Figure S6) for measurement at 260 K. Spectra are color coded as: H_{ox}, black; H_{red}', magenta; $H_{red}H^+$, green; H_{red}, blue; and H_{hyd}, red.

Temperature annealing was further used to probe the temperature-induced changes in the redox state population of NaDT reduced CaI (Figure 6 and Figure S6). This technique probes electronically coupled transitions by gradual warming of cryo-trapped intermediates.[46] The 13 K spectrum was composed of a mixture of H_{ox}, H_{red}', $H_{red}H^+$ and H_{hyd}, which upon annealing to 150 K led to the appearance of H_{red} (see Figure S6, 10 K versus 150 K spectrum). Warming the 13K sample to 260 K had the most significant effect on the overall spectral composition, the intensities of both H_{hyd} and $H_{red}H^+$ decreased (H_{hyd} was not detected) whereas H_{ox} and H_{red}' increased (Figure 6). Accumulation of H_{ox} results from the temperature effect on proton-transfer at the H-cluster, which increases as *T* increases above 150 K. This results in turnover of H_{red}, $H_{red}H^+$ and H_{hyd} and release of H_2 and formation of H_{ox}. Reduction of H_{ox} by NaDT at 260 K leads to formation H_{red}'. Thus, the steady-state equilibrium of CaI shifts from an enrichment of $H_{red}H^+$ and H_{hyd} observed at 10 K, towards more H_{ox} with increasing temperature to 260 K, and together with the result summarized in Figure 5 directly supports $H_{red}H^+$ as a catalytic intermediate in the H_2 evolution reaction in CaI.

Conclusions

The results from the IR analysis of CaI and CrHydA1 using H/D-isotope exchanged cryogenic spectral collection, as well as from temperature annealing experiments are summarized in Scheme 1. For the proton reduction reaction, we propose that the predominant catalytic mechanism for CaI initiates with H_{ox} that undergoes a PCET step to form $H_{red}H^+$,[23] consistent with our previous results (Scheme 1, blue arrow). For CrHydA1, this step can proceed by ET/PT process involving H_{red}' where the reducing equivalent is located on $[4Fe\text{-}4S]_H$ (Scheme 1, green arrows).[47] Electron-transfer coupled to intramolecular proton exchange converts $H_{red}H^+$ to H_{hyd}, and a second proton-transfer step leads to the release of H_2 to reform H_{ox}, thereby completing the catalytic cycle. Decoupling of proton- and electron-transfer steps can lead to other reduced states such as H_{red} or H_{sred}. Overall, the steps illustrated here emphasize a central role for $H_{red}H^+$ in coupling proton and electrons to the evolution of H_2.

Scheme 1. H-cluster transitions during catalysis.[a]

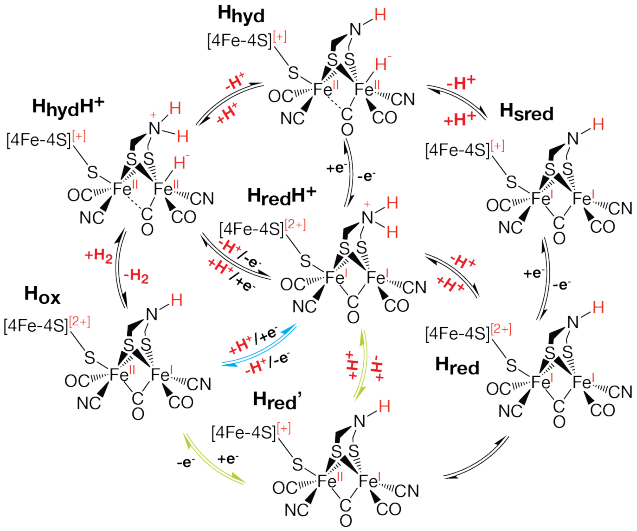

[a]H_{ox} is converted to $H_{red}H^+$ by PCET in CaI (blue arrow), and by ET/PT for CrHydA1 (green arrows). The μ-CO bridged H-cluster geometry is maintained throughout the catalytic cycle.

The contrasting models proposed for the μ-CO geometry and Fe_d coordination of the $H_{red}H^+$ state[13, 16, 25, 27, 29-30] thus have important implications on the reaction mechanism. The analysis of H-cluster geometries elicited from these results for CrHydA1 and CaI best support an H-cluster with a bridged μ-CO and a rotated $[2Fe]_H$ geometry for an accessible apical site on Fe_d.[48] This coordination geometry is also reproduced in DFT models of the proton reduction step by $[2Fe]_H$ compounds,[7, 13] distinguished by more favorable back-bonding from Fe_d into μ-CO, and would promote a more nucleophilic Fe_d for oxidative addition of a proton to form a hydride (e.g., $H_{red}H^+ \rightarrow H_{hyd}$). Moreover, this geometry enables PCET based H_2 activation chemistry with rapid proton exchange with adt. Therefore, a common μ-CO bridged geometry among catalytic states (i.e., H_{ox}, $H_{red}H^+$, and H_{hyd}) would necessitate minimal structural rearrangement of the H-cluster throughout catalysis to afford high reversibility

Pursuant to the DOE Public Access Plan, this document represents the authors' peer-reviewed, accepted manuscript. The published version of the article is available from the relevant publisher.

and fast catalytic rates by [FeFe] H_2ase CaI. These design principles may prove instrumental in the development of synthetic hydrogen activation catalysts.

ASSOCIATED CONTENT

Supporting Information

Materials and methods, table of CaI *ν*CN and *ν*CO band frequencies from IR spectra. FTIR spectra of: (i) CaI auto-oxidized, NaDT reduced in H_2O, and NaDT reduced in D_2O collected at 295 K; (ii) CrHydA1 auto-oxidized, reduced with H_2 in H_2O, and D_2 reduced in D_2O collected at 295 K, (iii) CrHydA1 auto-oxidized, D_2 reduced in D_2O, and the oxidized-reduced difference spectra collected at 295 K; (iv) NaDT reduced CrHydA1, CaI and CaI 298S variant collected at 10 K; (v) CaI reduced with H_2 in H_2O, D_2 in D_2O, NaDT in H_2O and NaDT in D_2O collected at 10 K.

The Supporting Information is available free of charge on the ACS Publications website.

AUTHOR INFORMATION

Corresponding Author

*paul.king@nrel.gov.

ACKNOWLEDGMENT

This work was authored in part by Alliance for Sustainable Energy, LLC, the manager and operator of the National Renewable Energy Laboratory for the U.S. Department of Energy (DOE) under Contract No. DE-AC36-08GO28308. Funding was provided by the U.S. Department of Energy Office of Basic Energy Sciences, Division of Chemical Sciences, Geosciences, and Biosciences. The views expressed in the article do not necessarily represent the views of the DOE or the U.S. Government. The U.S. Government and the publisher, by accepting the article for publication, acknowledges that the U.S. Government retains a nonexclusive, paid-up, irrevocable, worldwide license to publish or reproduce the published form of this work, or allow others to do so, for U.S. Government purposes.

REFERENCES

1. Adams, M. W. W., *Biochim. Biophys. Acta, Bioenergetics* **1990,** *1020*, 115-145.
2. Peters, J. W.; Schut, G. J.; Boyd, E. S.; Mulder, D. W.; Shepard, E. M.; Broderick, J. B.; King, P. W.; Adams, M. W., *Biochim. Biophys. Acta, Mol. Cell Res.* **2015,** *1853*, 1350-1369.
3. Przybyla, A. E.; Robbins, J.; Menon, N.; Peck, H. D., *FEMS Microbiol. Lett.* **1992,** *88*, 109-136.
4. Nicolet, Y.; Piras, C.; Legrand, P.; Hatchikian, C. E.; Fontecilla-Camps, J. C., *Structure* **1999,** *7*, 13-23.
5. Peters, J. W.; Lanzilotta, W. N.; Lemon, B. J.; Seefeldt, L. C., *Science* **1998,** *282*, 1853-1858.
6. Berggren, G.; Adamska, A.; Lambertz, C.; Simmons, T. R.; Esselborn, J.; Atta, M.; Gambarelli, S.; Mouesca, J. M.; Reijerse, E.; Lubitz, W.; Happe, T.; Artero, V.; Fontecave, M., *Nature* **2013,** *499*, 66-69.
7. Fan, H.-J.; Hall, M. B., *J. Am. Chem. Soc.* **2001,** *123*, 3828-3829.
8. Ryde, U.; Greco, C.; De Gioia, L., *J. Am. Chem. Soc.* **2010,** *132*, 4512-4513.
9. Cornish, A. J.; Ginovska, B.; Thelen, A.; da Silva, J. C. S.; Soares, T. A.; Raugei, S.; Dupuis, M.; Shaw, W. J.; Hegg, E. L., *Biochemistry* **2016,** *55*, 3165-3173.
10. Ginovska-Pangovska, B.; Ho, M.-H.; Linehan, J. C.; Cheng, Y.; Dupuis, M.; Raugei, S.; Shaw, W. J., *Biochim. Biophys. Acta, Bioenergetics* **2014,** *1837*, 131-138.
11. Long, H.; King, P. W.; Chang, C. H., *J. Phys. Chem. B* **2014,** *118*, 890-900.
12. Madden, C.; Vaughn, M. D.; Díez-Pérez, I.; Brown, K. A.; King, P. W.; Gust, D.; Moore, A. L.; Moore, T. A., *J. Am. Chem. Soc.* **2011,** *134*, 1577-1582.
13. Mulder, D. W.; Ratzloff, M. W.; Bruschi, M.; Greco, C.; Koonce, E.; Peters, J. W.; King, P. W., *J. Am. Chem. Soc.* **2014,** *136*, 15394-15402.
14. Winkler, M.; Senger, M.; Duan, J.; Esselborn, J.; Wittkamp, F.; Hofmann, E.; Apfel, U.-P.; Stripp, S. T.; Happe, T., *Nat. Commun.* **2017,** *8*, 16115.
15. Senger, M.; Mebs, S.; Duan, J.; Shulenina, O.; Laun, K.; Kertess, L.; Wittkamp, F.; Apfel, U.-P.; Happe, T.; Winkler, M., *Phys. Chem. Chem. Phys.* **2018,** *20*, 3128-3140.
16. Sommer, C.; Adamska-Venkatesh, A.; Pawlak, K.; Birrell, J. A.; Rüdiger, O.; Reijerse, E. J.; Lubitz, W., *J. Am. Chem. Soc.* **2017,** *139*, 1440-1443.
17. Adamska-Venkatesh, A.; Krawietz, D.; Siebel, J.; Weber, K.; Happe, T.; Reijerse, E.; Lubitz, W., *J. Am. Chem. Soc.* **2014,** *136*, 11339-11346.
18. Esselborn, J.; Lambertz, C.; Adamska-Venkatesh, A.; Simmons, T.; Berggren, G.; Noth, J.; Siebel, J.; Hemschemeier, A.; Artero, V.; Reijerse, E.; Fontecave, M.; Lubitz, W.; Happe, T., *Nat. Chem. Biol.* **2013,** *9*, 607-609.
19. Siebel, J. F.; Adamska-Venkatesh, A.; Weber, K.; Rumpel, S.; Reijerse, E.; Lubitz, W., *Biochemistry* **2015,** *54*, 1474-1483.
20. Knörzer, P.; Silakov, A.; Foster, C. E.; Armstrong, F. A.; Lubitz, W.; Happe, T., *J. Biol. Chem.* **2011,** *287*, 1489-1499.
21. Morra, S.; Maurelli, S.; Chiesa, M.; Mulder, D. W.; Ratzloff, M. W.; Giamello, E.; King, P. W.; Gilardi, G.; Valetti, F., *Biochim. Biophys. Acta, Bioenergetics* **2016,** *1857*, 98-106.
22. Mulder, D. W.; Guo, Y.; Ratzloff, M. W.; King, P. W., *J. Am. Chem. Soc.* **2017,** *139*, 83-86.
23. Ratzloff, M. W.; Wilker, M. B.; Mulder, D. W.; Lubner, C. E.; Hamby, H.; Brown, K. A.; Dukovic, G.; King, P. W., *J. Am. Chem. Soc.* **2017,** *139*, 12879-12882.
24. Pandey, A. S.; Harris, T. V.; Giles, L. J.; Peters, J. W.; Szilagyi, R. K., *J. Am. Chem. Soc.* **2008,** *130*, 4533-4540.
25. Nicolet, Y.; de Lacey, A. L.; Vernède, X.; Fernandez, V. M.; Hatchikian, E. C.; Fontecilla-Camps, J. C., *J. Am. Chem. Soc.* **2001,** *123*, 1596-1604.
26. Silakov, A.; Kamp, C.; Reijerse, E.; Happe, T.; Lubitz, W., *Biochemistry* **2009,** *48*, 7780-7786.
27. Mebs, S.; Senger, M.; Duan, J.; Wittkamp, F.; Apfel, U.-P.; Happe, T.; Winkler, M.; Stripp, S. T.; Haumann, M., *J. Am. Chem. Soc.* **2017,** *139*, 12157-12160.
28. Agnieszka, A.; Alexey, S.; Camilla, L.; Olaf, R.; Thomas, H.; Edward, R.; Wolfgang, L., *Angew. Chem., Int. Ed.* **2012,** *51*, 11458-11462.
29. Silakov, A.; Wenk, B.; Reijerse, E.; Lubitz, W., *PCCP.* **2009,** *11*, 6592-6599.
30. Chongdar, N.; Birrell, J. A.; Pawlak, K.; Sommer, C.; Reijerse, E. J.; Rüdiger, O.; Lubitz, W.; Ogata, H., *J. Am. Chem. Soc.* **2018,** *140*, 1057-1068.
31. Greco, C.; Bruschi, M.; Fantucci, P.; Ryde, U.; De Gioia, L., *J. Am. Chem. Soc.* **2011,** *133*, 18742-18749.
32. Artz, J. H.; Mulder, D. W.; Ratzloff, M. W.; Lubner, C. E.; Zadvornyy, O. A.; LeVan, A. X.; Williams, S. G.; Adams, M. W. W.; Jones, A. K.; King, P. W.; Peters, J. W., *J. Am. Chem. Soc.* **2017,** *139*, 9544-9550.
33. Rodríguez-Maciá, P.; Pawlak, K.; Rüdiger, O.; Reijerse, E. J.; Lubitz, W.; Birrell, J. A., *J. Am. Chem. Soc.* **2017,** *139*, 15122-15134.
34. Gauquelin, C.; Baffert, C.; Richaud, P.; Kamionka, E.; Etienne, E.; Guieysse, D.; Girbal, L.; Fourmond, V.; André, I.; Guigliarelli, B.; Léger, C.; Soucaille, P.; Meynial-Salles, I., *Biochim. Biophys. Acta, Bioenergetics* **2018,** *1859*, 69-77.
35. Therien, J. B.; Artz, J. H.; Poudel, S.; Hamilton, T. L.; Liu, Z.; Noone, S. M.; Adams, M. W. W.; King, P. W.; Bryant, D. A.; Boyd, E. S.; Peters, J. W., *Front Microbiol.* **2017,** *8*.
36. Liu, Y.-C.; Yen, T.-H.; Chu, K.-T.; Chiang, M.-H., *Comments Inorg. Chem.* **2016,** *36*, 141-181.
37. Rauchfuss, T. B., *Acc. Chem. Res.* **2015,** *48*, 2107-2116.

Pursuant to the DOE Public Access Plan, this document represents the authors' peer-reviewed, accepted manuscript. The published version of the article is available from the relevant publisher.

38. Apfel, U.-P.; Pétillon, F.; Schollhammer, P.; Talarmin, J.; Weigand, W., [FeFe] Hydrogenase Models: An Overview. In *Bioinspired Catalysis: Metal-Sulfur Complexes*, Weigand, W., Schollhammer, P., Ed. Wiley-VCH: Germany, 2014; pp 79-104.
39. Mulder, D. W.; Ratzloff, M. W.; Shepard, E. M.; Byer, A. S.; Noone, S. M.; Peters, J. W.; Broderick, J. B.; King, P. W., *J. Am. Chem. Soc.* **2013,** *135*, 6921-6929.
40. Birrell, J. A.; Wrede, K.; Pawlak, K.; Rodriguez-Maciá, P.; Rüdiger, O.; Reijerse, E. J.; Lubitz, W., *Isr. J. Chem.* **2016,** *56*, 852-863.
41. Roseboom, W.; Lacey, A. L.; Fernandez, V. M.; Hatchikian, E. C.; Albracht, S. P. J., *J. Biol. Inorg. Chem.* **2005,** *11*, 102-118.
42. Reijerse, E. J.; Pham, C. C.; Pelmenschikov, V.; Gilbert-Wilson, R.; Adamska-Venkatesh, A.; Siebel, J. F.; Gee, L. B.; Yoda, Y.; Tamasaku, K.; Lubitz, W.; Rauchfuss, T. B.; Cramer, S. P., *J. Am. Chem. Soc.* **2017,** *139*, 4306-4309.
43. Pelmenschikov, V.; Birrell, J. A.; Pham, C. C.; Mishra, N.; Wang, H.; Sommer, C.; Reijerse, E.; Richers, C. P.; Tamasaku, K.; Yoda, Y.; Rauchfuss, T. B.; Lubitz, W.; Cramer, S. P., *J. Am. Chem. Soc.* **2017,** *139*, 16894-16902.
44. King, P. W.; Svedruzic, D.; Hambourger, M.; Gervaldo, M.; McDonald, T.; Blackburn, J.; Heben, M.; Gust, D.; Moore, A. L.; Moore, T. A., *Solar Hydrogen and Nanotechnology II* **2007,** *6650*, 66500J.
45. Schilter, D.; Camara, J. M.; Huynh, M. T.; Hammes-Schiffer, S.; Rauchfuss, T. B., *Chem. Rev.* **2016,** *116*, 8693-8749.
46. Chapman, A.; Cammack, R.; Hatchikian, C. E.; McCracken, J.; Peisach, J., *FEBS Lett.* **1988,** *242*, 134-138.
47. Katz, S.; Noth, J.; Horch, M.; Shafaat, H.; Happe, T.; Hildebrandt, P.; Zebger, I., *Chem. Sci.* **2016,** *7*, 6746-6752.
48. Darensbourg, M. Y.; Lyon, E. J.; Zhao, X.; Georgakaki, I. P., *Proc. Natl. Acad. Sci. U. S. A.* **2003,** *100*, 3683-3688.

Pursuant to the DOE Public Access Plan, this document represents the authors' peer-reviewed, accepted manuscript. The published version of the article is available from the relevant publisher.

TOC graphic.

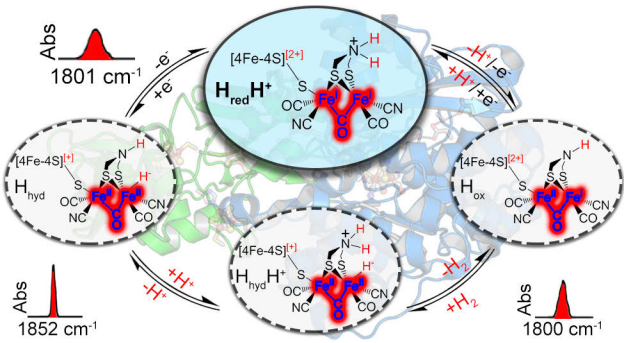

Pursuant to the DOE Public Access Plan, this document represents the authors' peer-reviewed, accepted manuscript. The published version of the article is available from the relevant publisher.